

Elsevier Editorial System(tm) for Agricultural and Forest Meteorology
Manuscript Draft

Manuscript Number: AGRFORMET-D-14-00328R2

Title: Estimation of crop gross primary production (GPP): II. Do scaled MODIS vegetation indices improve performance?

Article Type: Research Paper

Section/Category: Plant physiology, Crop Modelling, water relations including evapotranspiration, WUE, interception

Keywords: Daily GPP, MODIS, Vegetation Index, fAPARchl

Corresponding Author: Dr. Qingyuan Zhang, Ph.D.

Corresponding Author's Institution: USRA

First Author: Qingyuan Zhang, Ph.D.

Order of Authors: Qingyuan Zhang, Ph.D.; Yen-Ben Cheng; Alexei Lyapustin; Yujie Wang; Xiaoyang Zhang; Andrew Suyker; Shashi Verma; Yanmin Shuai; Elizabeth M Middleton

Abstract: Satellite remote sensing estimates of Gross Primary Production (GPP) have routinely been made using spectral Vegetation Indices (VIs) over the past two decades. The Normalized Difference Vegetation Index (NDVI), the Enhanced Vegetation Index (EVI), the green band Wide Dynamic Range Vegetation Index (WDRVIgreen), and the green band Chlorophyll Index (CIgreen) have been employed to estimate GPP under the assumption that GPP is proportional to the product of VI and photosynthetically active radiation (PAR) (where VI is one of four VIs: NDVI, EVI, WDRVIgreen, or CIgreen). However, the empirical regressions between VI*PAR and GPP measured locally at flux towers do not pass through the origin (i.e., the zero X-Y value for regressions). Therefore they are somewhat difficult to interpret and apply. This study investigates (1) what are the scaling factors and offsets (i.e., regression slopes and intercepts) between the fraction of PAR absorbed by chlorophyll of a canopy (fAPARchl) and the VIs, and (2) whether the scaled VIs developed in (1) can eliminate the deficiency and improve the accuracy of GPP estimates. Three AmeriFlux maize and soybean fields were selected for this study, two of which are irrigated and one is rainfed. The four VIs and fAPARchl of the fields were computed with the MODerate resolution Imaging Spectroradiometer (MODIS) satellite images. The GPP estimation performance for the scaled VIs was compared to results obtained with the original VIs and evaluated with standard statistics: the coefficient of determination (R^2), the root mean square error (RMSE), and the coefficient of variation (CV). Overall, the scaled EVI obtained the best performance. The performance of the scaled NDVI, EVI and WDRVIgreen was improved across sites, crop types and soil/background wetness conditions. The scaled CIgreen did not improve results, compared to the original CIgreen. The scaled green band indices (WDRVIgreen, CIgreen) did not exhibit superior performance to either the scaled EVI or NDVI in estimating crop daily GPP at these agricultural fields. The scaled VIs are more physiologically meaningful than original un-scaled VIs, but scaling factors and offsets may vary across crop types and surface conditions.

Highlights

- Scale factor and offset are derived with linear regression of $fAPAR_{chl}$ vs. VI
- Scaled NDVI, EVI and $WDRVI_{green}$ improve performance
- Scaled EVI exhibits the best performance
- Scale factor and offset vary with crop types and surface conditions

1 Estimation of crop gross primary production (GPP):

2 II. Do scaled MODIS vegetation indices improve performance?

3 Qingyuan Zhang^{1,2}, Yen-Ben Cheng^{3,2}, Alexei I. Lyapustin⁴, Yujie Wang^{5,2}, Xiaoyang Zhang⁶,
4 Andrew Suyker⁷, Shashi Verma⁷, Yanmin Shuai⁸, Elizabeth M. Middleton²

5

6 ¹Universities Space Research Association, Columbia, MD 21044, USA

7 ²Biospheric Sciences Laboratory, National Aeronautics and Space Administration/Goddard Space
8 Flight Center, Greenbelt, MD 20771, USA

9 ³Sigma Space Corporation, Lanham, MD 20706, USA

10 ⁴Climate and Radiation Laboratory, Code 613, National Aeronautics and Space Administration
11 Goddard Space Flight Center, Greenbelt, MD 20771, USA

12 ⁵Goddard Earth Sciences and Technology Center, University of Maryland Baltimore County,
13 Baltimore, MD 21228, USA

14 ⁶Geospatial Sciences Center of Excellence, South Dakota State University, Brookings, SD 57007,
15 USA

16 ⁷School of Natural Resources, University of Nebraska—Lincoln, Lincoln, NE 68588, USA

17 ⁸Earth Resources Technology, Inc., Laurel, MD 20707, USA

18

19

20 Corresponding author:

21 Qingyuan Zhang

22 Address:

23 Building 33, Room G317

24 Biospheric Sciences Laboratory, Code 618,

25 NASA/Goddard Space Flight Center,

26 Greenbelt, Maryland 20771, USA

27

28 Email: qyz72@yahoo.com

29

30

31 **Abstract** –Satellite remote sensing estimates of Gross Primary Production (GPP) have routinely
32 been made using spectral Vegetation Indices (VIs) over the past two decades. The Normalized
33 Difference Vegetation Index (NDVI), the Enhanced Vegetation Index (EVI), the green band
34 Wide Dynamic Range Vegetation Index ($WDRVI_{green}$), and the green band Chlorophyll Index
35 (CI_{green}) have been employed to estimate GPP under the assumption that GPP is proportional to
36 the product of VI and photosynthetically active radiation (PAR) (where VI is one of four VIs:
37 NDVI, EVI, $WDRVI_{green}$, or CI_{green}). However, the empirical regressions between VI*PAR and
38 GPP measured locally at flux towers do not pass through the origin (i.e., the zero X-Y value for
39 regressions). Therefore they are somewhat difficult to interpret and apply. This study
40 investigates (1) what are the scaling factors and offsets (i.e., regression slopes and intercepts)
41 between the fraction of PAR absorbed by chlorophyll of a canopy ($fAPAR_{chl}$) and the VIs, and (2)
42 whether the scaled VIs developed in (1) can eliminate the deficiency and improve the accuracy
43 of GPP estimates. Three AmeriFlux maize and soybean fields were selected for this study, two of
44 which are irrigated and one is rainfed. The four VIs and $fAPAR_{chl}$ of the fields were computed
45 with the MODerate resolution Imaging Spectroradiometer (MODIS) satellite images. The GPP
46 estimation performance for the scaled VIs was compared to results obtained with the original VIs
47 and evaluated with standard statistics: the coefficient of determination (R^2), the root mean
48 square error (RMSE), and the coefficient of variation (CV). Overall, the scaled EVI obtained the
49 best performance. The performance of the scaled NDVI, EVI and $WDRVI_{green}$ was improved
50 across sites, crop types and soil/background wetness conditions. The scaled CI_{green} did not
51 improve results, compared to the original CI_{green} . The scaled green band indices ($WDRVI_{green}$,
52 CI_{green}) did not exhibit superior performance to either the scaled EVI or NDVI in estimating crop
53 daily GPP at these agricultural fields. The scaled VIs are more physiologically meaningful than

54 original un-scaled VIs, but scaling factors and offsets may vary across crop types and surface
55 conditions.

56 **Key Words – Daily GPP, MODIS, Vegetation Index, fAPAR_{chl}**

57

58 I. INTRODUCTION

59 Atmospheric general circulation models require quantification of land-atmosphere
60 exchanges of energy, water and momentum, including CO₂ fluxes which can be provided by land
61 surface process models (Bonan et al., 2011; Dickinson et al., 1993; Sellers et al., 1986). Satellite
62 remote sensing offers inputs such as land cover types and the Normalized Difference Vegetation
63 Index (NDVI) (Deering, 1978; Tucker, 1979) for use in the land surface modeling (Dickinson et
64 al., 1990; Sellers et al., 1994). Pioneering work (Asrar et al., 1992; Myneni et al., 1997; Running
65 et al., 2000; Sellers, 1987) has shown the fraction of photosynthetically active radiation (PAR)
66 absorbed by a canopy/vegetation (FPAR, i.e., fAPAR_{canopy}) can be approximated with NDVI
67 (Running et al., 2000). Therefore, NDVI has been employed to estimate vegetation Gross
68 Primary Productivity (GPP) in a variation (as $GPP = \epsilon * NDVI * PAR$, Running et al., 2000),
69 inspired by the logic from the Light Use Efficiency (LUE) model (Monteith, 1972, 1977):

$$70 \quad GPP = \epsilon * fAPAR_{PSN} * PAR = \epsilon * APAR_{PSN}, \quad (1)$$

71 where ϵ is LUE for vegetation photosynthesis (PSN) (Running et al., 2000) and fAPAR_{PSN} is the
72 fraction of PAR absorbed for PSN (APAR_{PSN}). Monitoring changes in crop GPP with satellite
73 remote sensing data advances the capability to understand and manage global food security,
74 sustainability practices, and environmental impacts, and to study global carbon cycle and global
75 water cycle.

76 The three-band Enhanced Vegetation Index (EVI) (Huete et al., 1997) and the two-band
77 EVI (called EVI2, Jiang et al., 2008) have also been utilized to predict terrestrial GPP in a
78 similar way as $GPP = \epsilon * EVI * PAR$ (Jin et al., 2013; Kalfas et al., 2011; King et al., 2011; Li et al.,
79 2007; Mahadevan et al., 2008; Schubert et al., 2012; Sjöström et al., 2011; Wu et al., 2008, 2010,
80 2011, 2012; Xiao et al., 2004; Yan et al., 2009). In addition, Gitelson and colleagues also
81 explored the application of the green band Wide Dynamic Range Vegetation Index ($WDRVI_{green}$)
82 and the green band Chlorophyll Index (CI_{green}) for crop GPP estimation, in addition to the NDVI
83 and EVI (Gitelson et al., 2008, 2012; Peng and Gitelson, 2011, 2012; Peng et al., 2011).

84 However, since the empirical regressions between the $VI * PAR$ products and GPP
85 measured locally at flux towers do not pass through the origin (i.e., the zero X-Y value for
86 regressions) and produce offsets, they are somewhat difficult to interpret and apply (Gitelson et
87 al., 2012; Sims et al., 2006; Zhang et al., 2014b). This is considered to be a source of error
88 affecting the accuracy and reliability of remote sensing GPP estimates based on VIs. In the
89 literature, there is no paper that presents how to scale the VIs in space and time to solve the
90 problem.

91 The standard MODerate resolution Imaging Spectroradiometer (MODIS) 8-day GPP
92 product (MOD17A2 GPP) uses the MOD15A2 FPAR (a $fAPAR_{canopy}$) product as a model input
93 (Running et al., 2004; Zhao and Running, 2008). Investigations to find the scaling factor and
94 offset of NDVI through $fAPAR_{canopy} - NDVI$ functions have been conducted, where $fAPAR_{canopy}$
95 $= a_0 * NDVI + b_0$ (a_0 is the scaling factor or slope, and b_0 is y intercept or offset) (Fensholt et al.,
96 2004; Goward and Huemmrich, 1992; Knyazikhin et al., 1998, 2002; Potter et al., 1993; Prince
97 and Goward, 1995; Randerson et al., 1996; Sellers et al., 1996; Sims et al., 2005). However, the
98 MOD15A2 FPAR product overestimates *in-situ* $fAPAR_{canopy}$ during spring greenup and fall

99 senescent periods, and underestimates *in-situ* $fAPAR_{canopy}$ in mid-summer during peak GPP
100 activity at the agricultural fields we selected [see (Zhang et al., 2014a) for details].

101 We developed an algorithm to retrieve the fraction of PAR absorbed by chlorophyll
102 throughout the canopy ($fAPAR_{chl}$) from actual MODIS observations or from synthesized 30 m
103 MODIS-spectral-like observations simulated with EO-1 Hyperion images (Zhang, 2003; Zhang
104 et al., 2005, 2009, 2012, 2013,2014c). We found that $fAPAR_{chl} \neq fAPAR_{canopy}$, and that the
105 fraction of PAR absorbed by foliage non-chlorophyll components ($fAPAR_{non-chl}$) varies with
106 types and seasonally (Zhang et al., 2013). Zhang et al. (2014a) presented the performance of
107 $fAPAR_{chl}$ and MOD15A2 FPAR in crop GPP estimation, and concluded that $fAPAR_{chl}$ is
108 superior to MOD15A2 FPAR. Zhang et al. (2014b) investigated the performance of original un-
109 scaled VIs in GPP estimation, and suggested that further investigation on the performance of
110 scaled VIs should be carried out.

111 The objectives of this paper are straightforward: 1] to explore how surface conditions
112 affect the scaling factors (“a”) and offsets (“b”) derived through regression analysis of $fAPAR_{chl}$
113 vs. the four VIs: $fAPAR_{chl} = a * VI + b$ for each crop type (corn, soybean) per field; 2] to investigate
114 how much the scaled VIs can improve the prediction accuracy of GPP estimates compared to the
115 prediction of original un-scaled VIs.

116

117

II. METHODS

II.1 Study sites and tower data

118 The three AmeriFlux crop sites for corn, or maize (*Zea mays* L.) and soybean (*Glycine*
119 *max* [L.] Merr.) used in this study are located at the University of Nebraska–Lincoln (UNL)

120

121 Agricultural Research and Development Center near Mead, Nebraska (US-NE1, US-NE2 and
122 US-NE3). The first two fields are circular (radius ~ 390 m) and equipped with center-pivot
123 irrigation systems (US-NE1, 41°09'54.2"N, 96°28'35.9"W; US-NE2, 41°09'53.6"N,
124 96°28'07.5"W). The third is a 790 m long square field (US-NE3, 41°10'46.7"N,
125 96°26'22.4"W) that relies entirely on rainfall. Each field is equipped with an eddy covariance
126 flux tower (Gitelson et al., 2012; Gitelson et al., 2006; Peng et al., 2013). The first field (US-NE1)
127 is a continuous maize field while the other two fields are maize-soybean rotation fields (soybean
128 is planted in even years).

129 Tower eddy-covariance carbon exchange, PAR, and GPP measurements in growing
130 season from 2001- 2006 are publically available and can be downloaded from
131 <ftp://cdiac.ornl.gov/pub/ameriflux/data>. The nighttime ecosystem respiration/temperature Q_{10}
132 relationship was used to estimate the daytime ecosystem respiration (Baldocchi, 2003). Daily
133 GPP was computed by subtracting respiration (R) from net ecosystem exchange (NEE), i.e.,
134 $GPP=NEE-R$ (Suyker et al., 2005). These sites provided the opportunity to examine the semi-
135 empirical relationships between $fAPAR_{chl}$ versus VIs for both C4 (maize) and C3 (soybean)
136 crops in both irrigated and non-irrigated ecosystems, and to investigate the benefits of employing
137 the scaled relationships to estimate GPP.

138 **II.2 Remote sensing data processing and GPP estimation**

139 Six years (2001-2006) of MODIS L1B calibrated radiance data (MOD021KM and
140 MOD02HKM) and geolocation data (MOD03) covering the three study sites were downloaded
141 from <https://ladsweb.nascom.nasa.gov:9400/data/>. Two of the MODIS bands have a nadir spatial
142 resolution of 250 m: B1 (red, 620 – 670 nm) and B2 (near infrared, NIR₁, 841 – 876 nm). The
143 MODIS land bands 3 - 7 have a nadir spatial resolution of 500 m: B3 (blue, 459 – 479 nm), B4

144 (green, 545 – 565 nm), B5 (NIR₂, 1230 – 1250 nm), B6 (shortwave infrared, SWIR₁, 1628 –
145 1652 nm) and B7 (SWIR₂, 2105 – 2155 nm). The centers of the original 500 m grids defined in
146 the standard surface reflectance product (MOD09) that encompass the three tower sites are not
147 the centers of the three fields and vegetation in each of the original 500 m grids is not
148 homogeneous [see Figure 2 of (Guindin-Garcia et al., 2012)]. The MODIS gridding procedure
149 for the standard MOD09 product does not ensure the gridded surface reflectance covers the
150 entire grid (Wolfe et al., 1998). A modified gridding procedure was used for this study (Zhang et
151 al., 2014b), whereby the centers of the three 500 m grids were matched to the centers of the three
152 fields, respectively. The L1B radiance data from each swath were gridded at 500 m resolution for
153 MODIS bands 1-7 with area weight of each MODIS observation. This modified gridding
154 processing was incorporated into the Multi-Angle Implementation of Atmospheric Correction
155 (MAIAC) algorithm (Lyapustin et al., 2008, 2011a, b, 2012). MAIAC is an advanced algorithm
156 which uses time series analysis and a combination of pixel-based and image-based processing to
157 improve cloud/snow detection, and to achieve more accurate aerosol retrievals and atmospheric
158 correction, based on the bidirectional reflectance distribution function (BRDF) model of the
159 surface.

160 Derived bidirectional reflectance factors (BRF, also called directional surface reflectance)
161 in MODIS bands 1-7 were used for this study. The impact of MODIS observation footprint size
162 resulting from variable view zenith angle (VZA) on crop daily GPP estimation for these sites
163 was recently reported elsewhere (Zhang et al., 2014b). In order to eliminate the potential bias due
164 to large VZAs, only observations with $VZA \leq 35^\circ$ were included in this study. The surface
165 reflectance data (ρ) were used to calculate the following indices (Deering, 1978; Gitelson, 2004;
166 Gitelson et al., 2007, 2012; Huete et al., 1997, 2002; Tucker, 1979):

$$167 \quad CI_{green} = \frac{\rho_{NIR_1} - 1}{\rho_{green}} \quad (2)$$

$$168 \quad WDRVI_{green} = \frac{0.3\rho_{NIR_1} - \rho_{green}}{0.3\rho_{NIR_1} + \rho_{green}} + \frac{1-0.3}{1+0.3} \quad (3)$$

$$169 \quad NDVI = \frac{\rho_{NIR_1} - \rho_{red}}{\rho_{NIR_1} + \rho_{red}} \quad (4)$$

$$170 \quad EVI = 2.5 \frac{\rho_{NIR_1} - \rho_{red}}{1 + \rho_{NIR_1} + 6\rho_{red} - 7.5\rho_{blue}} \quad (5)$$

171 We used the PROSAIL2 model (Jacquemoud and Baret, 1990; Baret and Fourty, 1997;
 172 Braswell et al., 1996; Verhoef, 1984, 1985; Zhang et al., 2005, 2009, 2012, 2013), a coupled
 173 soil-canopy-leaf radiative transfer model, to retrieve $fAPAR_{chl}$, the fraction of PAR absorbed by
 174 the foliage of the canopy ($fAPAR_{foliage}$), and the fraction of PAR absorbed by the non-
 175 photosynthetic foliage components ($fAPAR_{non-chl}$)(Zhang et al., 2014a). A pixel is composed of
 176 canopy and soil (Zhang et al., 2009, 2012, 2013). The canopy is partitioned into foliage and stem
 177 (including branch), and the foliage component is further partitioned into chlorophyll (chl) and
 178 non-chlorophyll (non-chl) components, where non-chl is composed of non-photosynthetic
 179 pigments (referred to as brown pigment) and dry matter (Baret and Fourty, 1997). The surface
 180 reflectances of MODIS bands 1 – 7 are used for retrieval of $fAPAR$ variables (Zhang et al., 2009,
 181 2012, 2013, 2014c):

$$182 \quad fAPAR_{non-chl} = fAPAR_{brown_pigment} + fAPAR_{dry_matter} \quad (6)$$

$$183 \quad fAPAR_{foliage} = fAPAR_{chl} + fAPAR_{non-chl} \quad (7)$$

$$184 \quad fAPAR_{canopy} = fAPAR_{foliage} + fAPAR_{stem} \quad (8)$$

185 The scaling factors (“a”) and offsets (“b”) of VIs were derived from linear regression through
186 $fAPAR_{chl} - VI$ functions for each crop type per field, where $fAPAR_{chl} = a*VI + b$ (VIs=NDVI,
187 EVI, $WDRVI_{green}$, and CI_{green}).

188 The product of VIs and tower daily PAR ($VI*PAR$) and the product of scaled VIs and
189 daily PAR (scaled $VI*PAR$) were compared against the tower daily GPP for each crop type per
190 field ($GPP = \bar{\varepsilon}_0 * VI * PAR$ or $GPP = \bar{\varepsilon} * scaled\ VI * PAR$). The coefficients “ $\bar{\varepsilon}_0$ ” and “ $\bar{\varepsilon}$ ” were
191 computed with a least squares best fit algorithm. The computed values for $\bar{\varepsilon}_0$ and $\bar{\varepsilon}$ were then
192 used to predict GPP, and coefficient of determination (R^2), the root mean square error (RMSE, g
193 $C\ m^{-2}\ d^{-1}$) and coefficient of variation (CV, %) was calculated. The average light use efficiency
194 at chlorophyll level (LUE_{chl} , i.e., $\overline{\varepsilon_{chl}}$) was computed using $GPP = LUE_{chl} * fAPAR_{chl} * PAR$ with a
195 least squares best fit algorithm. Improvements of crop daily GPP estimation using scaled VIs
196 were assessed.

197

198

III. RESULTS

199 The scaling factor (“a”, also called slope) and offset (“b”, also called y-intercept)
200 obtained through the regression functions $fAPAR_{chl} = a*VI + b$ for each crop per field are listed in
201 Table 1, where the statistics for the R^2 , RMSE and x-intercept are also summarized. The x-
202 intercepts of $fAPAR_{chl} = a*VI + b$ give minimum VI values at zero $fAPAR_{chl}$. The 95% confidence
203 intervals of slope, y-intercept and x-intercept for each crop per field are reported, too. The CI_{green}
204 is a simple ratio index while the other three VIs include consideration of normalization. The
205 confidence intervals for CI_{green} are different from those for other three VIs for each type per field.
206 For each crop type in irrigated fields USNE1 and USNE2, the confidence intervals of y-
207 intercepts and x-intercepts for NDVI, EVI and CI_{green} are different from each other. For each

208 crop type in rainfed field USNE3, the confidence intervals of y-intercepts and x-intercepts for
209 NDVI and CI_{green} overlap each other, but are different from those for EVI. Mean values of the
210 confidence intervals of the slopes, y-intercepts and x-intercepts vary with VIs, sites, crop types
211 and irrigation options. None of the y-intercepts or x-intercepts for NDVI, EVI or $WDRVI_{\text{green}}$ is
212 close to the origin (i.e., zero X-Y point).

213 The functions in Tab. 1 were used to compute the scaled values of NDVI, EVI,
214 $WDRVI_{\text{green}}$ and CI_{green} for each crop type per field. For instance, for the NDVI at US-NE1:
215 scaled NDVI = $1.11 * NDVI - 0.29$. The coefficients $\bar{\varepsilon}_0$ and $\bar{\varepsilon}$ and LUE_{chl} of each crop per field are
216 listed in Table 2. Corn LUE_{chl} is ~1.6 times of soybean LUE_{chl} (Tab. 2), which agrees with the
217 expectation that C4 plants have higher LUE than C3 plants (e.g., Prince, 1991), and explains why
218 maize displays a wider daily GPP range ($\sim 34 \text{ g C m}^{-2} \text{ d}^{-1}$) than soybean ($\sim 19 \text{ g C m}^{-2} \text{ d}^{-1}$) (Zhang
219 et al., 2014b). The coefficients $\bar{\varepsilon}_0$ and $\bar{\varepsilon}$ were applied to estimate crop daily GPP.

220 Figure 1 shows the estimated soybean daily GPP for the rainfed field US-NE3 using the
221 four original VIs with $\bar{\varepsilon}_0$ and the scaled VIs with $\bar{\varepsilon}$, compared to tower daily GPP. The scaled
222 NDVI, EVI and $WDRVI_{\text{green}}$ combined with $\bar{\varepsilon}$ had better GPP estimation performance than the
223 original counterparts, respectively, demonstrating higher R^2 and lower RMSE. Compared to the
224 original counterparts, the (scaled NDVI)*PAR, the (scaled EVI)*PAR and the (scaled
225 $WDRVI_{\text{green}}$)*PAR values were closer to 0 when GPP=0. The scaled CI_{green} did not provide
226 better GPP estimation than the original CI_{green} . In order to save pages, similar figures for US-NE1,
227 US-NE2 and figures for maize in US-NE3 are not presented in this paper.

228 Table 3 summarized the statistics (R^2 , RMSE and CV) for estimating crop daily GPP
229 using the original VIs with $\bar{\varepsilon}_0$ and the scaled VIs with $\bar{\varepsilon}$, respectively. These statistics show that

230 the best performance was obtained with the scaled EVI while the least successful performance
231 among the four scaled VIs was obtained with CI_{green} across the sites, crop types and irrigation/
232 rainfed options. For example at the US-NE1 site, scaled EVI and scaled CI_{green} had contrasting
233 best/worst performances in GPP estimation: R^2 : 0.88/ 0.77, RMSE: 2.92/4.05 g C m⁻² d⁻¹, and
234 CV: 19%/ 26% (Tab. 3). GPP estimates for corn had better performance than for soybean using
235 scaled NDVI and EVI for sites US-NE2 and US-NE3. Better results might be achieved for the
236 sites examined in other studies (King et al., 2011; Sjöström et al., 2009) if the scaled EVI
237 (through coefficients obtained from the regression of $fAPAR_{chl}$ vs. EVI) had been utilized.

238 For each crop in any field, the scaled NDVI, EVI and $WDRVI_{green}$ improved the
239 prediction performance of crop daily GPP while the scaled CI_{green} did not, compared to the
240 original un-scaled VIs. GPP improvements for the three that benefited from scaling, ranked from
241 most to least were the NDVI, $WDRVI_{green}$, EVI, for which the R^2 increased (\uparrow : 0.16, 0.13, 0.09),
242 RMSE decreased (\downarrow :0.95, 0.78, 0.65 g C m⁻² d⁻¹), and the CV also decreased (\downarrow :8%, 6%, 5%).
243 The improvements also varied with crop types and irrigation conditions. For example, the NDVI
244 improvement for soybean (R^2 , \uparrow 0.20; CV, \downarrow 9%) was better than for corn (R^2 , \uparrow 0.13; CV, \downarrow 7%),
245 and the average improvement for the rainfed field (R^2 , \uparrow 0.21; RMSE, \downarrow 1.10 g C m⁻² d⁻¹; and CV,
246 \downarrow 10%) was better than for the irrigation fields (R^2 , \uparrow 0.12; RMSE, \downarrow 0.85 g C m⁻² d⁻¹; and
247 CV, \downarrow 6%).

248

249 IV. DISCUSSION

250 The PSROAIL2 model well distinguishes vegetation from soil and $fAPAR_{chl}$ retrieved
251 with the PROSAIL2 model excludes the impact of soil/background (Zhang et al., 2012, 2013).

252 The $fAPAR_{\text{foliage}}$ comprises chlorophyll and non-chlorophyll foliage fractions ($fAPAR_{\text{chl}}$,
253 $fAPAR_{\text{non-chl}}$). Therefore, the PAR absorbed by non-photosynthetic vegetation components (NPV)
254 of the canopy is excluded from $APAR_{\text{chl}}$ since $APAR_{\text{chl}} = fAPAR_{\text{chl}} * PAR$. This is the theoretical
255 basis for potential improvement of GPP estimation using the scaled VIs. The x-intercept values
256 of the semi-empirical linear functions of $fAPAR_{\text{chl}}$ vs. VI in Table 1 have an important
257 biophysical meaning: there is not any chlorophyll showing up at the pixel when its un-scaled VI
258 is less than its x-intercept value. Gitelson and colleagues (Gitelson et al., 2007) reported that,
259 before green-up when green leaves do not appear, MODIS 250 m NDVI values for the fields
260 could be greater than 0.2, which is close to the minimum x-intercepts of NDVI (0.23, Tab. 1) we
261 found with MODIS 500 m images. In irrigated fields, the mean values of the x-intercept
262 confidence intervals for EVI were about half of those for NDVI, and about 1/3 as large as those
263 for $WDRVI_{\text{green}}$ (Tab. 1). In rainfed fields, the mean values of the x-intercept confidence
264 intervals for EVI were about half of those for both NDVI and $WDRVI_{\text{green}}$ (Tab. 1).
265 Soil/background wetness has less impact on EVI than on NDVI which is consistent with the
266 original idea that inspired the development of EVI (Huete, 1988; Huete et al., 1997). Daughtry et
267 al. (2000) has expressed that VIs combined with NIR and red bands are less impacted by
268 background than VIs combined with NIR and green bands. Earlier studies (Sims et al., 2006,
269 2008) have shown that GPP drops to zero at variable EVI values (i.e., x-intercept EVI values) in
270 their selected flux sites, and have found the minimum x-intercept value is ~ 0.1 . So Sims et al.
271 (2008) has developed a GPP model using $EVI - 0.1$ instead of the original EVI. The x-intercept
272 confidence intervals of EVI in the three fields (US-NE1, US-NE2 and US-NE3) ranged from
273 (0.12, 0.13), (0.14, 0.15) to (0.16, 0.18). Our findings are consistent with earlier empirical studies
274 (Daughtry et al., 2000; Huete, 1988; Huete et al., 1997; Sims et al., 2006, 2008). Furthermore,

275 the scaled VIs with scaling factors and offsets using the semi-empirical relationships between
276 $fAPAR_{chl}$ vs. VIs for each crop type per field are more physiologically meaningful (Tab. 1) than
277 the original un-scaled VIs.

278 The $\bar{\epsilon}$ estimates for all scaled VIs are close to the relevant LUE_{chl} values for each crop
279 type per field. In contrast, the $\bar{\epsilon}_0$ estimates associated with the original un-scaled NDVI and
280 $WDRVI_{green}$ are lower than the relevant LUE_{chl} values. The $\bar{\epsilon}_0$ estimates for CI_{green} are much
281 lower than the relevant LUE_{chl} values because the original un-scaled CI_{green} range (~1 to 10) is
282 much wider than the scaled CI_{green} range (~0 to ~1). It is worth noting that both the $\bar{\epsilon}_0$ and the $\bar{\epsilon}$
283 estimates for the original EVI and the scaled EVI are close to the physiologically relevant LUE_{chl}
284 values. This partly explains the reasonableness and success of the Vegetation Photosynthesis
285 Model (VPM) (Xiao et al., 2004) which assumes $GPP = \epsilon * EVI * PAR$. This study suggests that the
286 GPP estimation made with the VPM may be improved by replacing the original EVI with
287 $fAPAR_{chl}$, or by scaling the EVI using the relationship between $fAPAR_{chl}$ and EVI.

288 The R^2 between tower daily GPP and estimated GPP with scaled VIs for all cases ranges
289 from 0.66 to 0.88 while the RMSE (CV) between them ranges from 4.37 to 2.11 $g\ C\ m^{-2}\ d^{-1}$
290 (from 31% to 17%). Although the R^2 between $fAPAR_{chl}$ and scaled VI is high for all cases (0.73
291 – 0.97), the RMSE between $fAPAR_{chl}$ and scaled VI varies with crop type, irrigation/rainfed
292 options, and VI options, which caused the variation of the performance of estimated GPP with
293 scaled VIs. Among the four scaled VIs, the RMSE between $fAPAR_{chl}$ and the scaled EVI is
294 smallest and the R^2 is highest for all study sites. For US-NE2 and US-NE3, the RMSE between
295 $fAPAR_{chl}$ and scaled CI_{green} is biggest and the R^2 is lowest.

296

V. CONCLUSION

297
298 This study exhibited improvement in the performance of crop daily GPP estimation using
299 scaled NDVI, EVI and $WDRVI_{green}$, compared to their original un-scaled counterparts. However,
300 performance improvement of crop daily GPP estimation using scaled CI_{green} was not observed.
301 The irrigated fields have better performance, as compared to the rainfed field. The performance
302 also varied with crop types and VI options. The scaled EVI provided the best performance
303 among all cases. This study does not find that the scaled $WDRVI_{green}$ or the scaled CI_{green} is
304 superior to the scaled NDVI or scaled EVI in predicting crop daily GPP.

305 Compared to the original VIs, the scaled VIs developed with the semi-empirical
306 relationships between $fAPAR_{chl}$ and VIs are more physiologically meaningful. However, the
307 scaling factors and offsets (and x-intercepts) vary field by field, and vary type by type.
308 Investigations to explore the scaling factors and offsets of these VIs using $fAPAR_{chl}$ for other
309 plant functional types should be carried out in the future. We will explore how the scaling factors
310 and offsets change over space and time, and vary with climate. Investigations on whether scaled
311 EVI is best for all fields and all types among the four scaled VIs are also needed. We suggest an
312 approach whereby MODIS-derived VIs are scaled pixel by pixel. This approach provides scaled
313 VIs for use when $fAPAR_{chl}$ is unavailable. We expect that future research on GPP simulation
314 based on the biochemical or land surface modeling (Bounoua et al., 2000; Potter et al., 2003;
315 Sellers et al., 1994, 1996) will achieve reduced uncertainty and improved accuracy when the
316 scaled MODIS VIs replace the original VIs.

ACKNOWLEDGMENTS

318 This study was supported by NASA Terrestrial Ecology project (Grant No., NNX12AJ51G; PI,
319 Q. Zhang) and NASA Science of Terra and Aqua project (Grant No., NNX14AK50G; PI, Q.
320 Zhang) (Dr. Diane Wickland, manager). We would like to thank the support and the use of
321 facilities and equipment provided by the Center for Advanced Land Management Information
322 Technologies and the Carbon Sequestration program, University of Nebraska–Lincoln. Site-
323 specific climate and CO₂ flux data are distributed by AmeriFlux network
324 (<http://public.ornl.gov/ameriflux>), supported by Carbon Dioxide Information Analysis Center at
325 the Oak Ridge National Laboratory of the Department of Energy. We are grateful to anonymous
326 reviewers whose comments helped improve the paper.

327

328 **References:**

- 329 Asrar, G., Myneni, R.B., & Choudhury, B.J. (1992). Spatial Heterogeneity in Vegetation
330 Canopies and Remote-Sensing of Absorbed Photosynthetically Active Radiation - a
331 Modeling Study. *Remote Sensing of Environment*, 41, 85-103
- 332 Baldocchi, D.D. (2003). Assessing the eddy covariance technique for evaluating carbon dioxide
333 exchange rates of ecosystems: past, present and future. *Global Change Biol.*, 9, 479-492
- 334 Bonan, G.B., Lawrence, P.J., Oleson, K.W., Levis, S., Jung, M., Reichstein, M., Lawrence, D.M.,
335 & Swenson, S.C. (2011). Improving canopy processes in the Community Land Model
336 version 4 (CLM4) using global flux fields empirically inferred from FLUXNET data.
337 *Journal of Geophysical Research*, 116, G02014
- 338 Baret, F., & Fourty, T. (1997). Radiometric estimates of nitrogen status in leaves and canopies.
339 In G. Lemaire (Ed.), *Diagnosis of the nitrogen status in crops* (pp. 201–227). Berlin,
340 Springer.
- 341 Bounoua, L., Collatz, G.J., Los, S.O., Sellers, P.J., Dazlich, D.A., Tucker, C.J., & Randal, D.A.
342 (2000). Sensitivity of Climate to Changes in NDVI. *Journal of Climate*, 13, 2277-2292
- 343 Braswell, B. H., Schimel, D. S., Privette, J. L., Moore, B., Emery, W. J., Sulzman, E. W., et al.
344 (1996). Extracting ecological and biophysical information from AVHRR optical data: An
345 integrated algorithm based on inverse modeling. *Journal of Geophysical Research-*
346 *Atmospheres*, 101, 23335–23348
- 347 Daughtry, C.S.T., Walthall, C.L., Kim, M.S., de Colstoun, E.B., & McMurtrey, J.E. (2000).
348 Estimating corn leaf chlorophyll concentration from leaf and canopy reflectance. *Remote*
349 *Sensing of Environment*, 74, 229-239
- 350 Deering, D.W. (1978). Rangeland reflectance characteristics measured by aircraft and spacecraft
351 sensors. In, *College Station* (p. 338). TX: Texas A&M University

352 Dickinson, R.E., A. Henderson-Sellers, & Kennedy, P.J. (1993). Biosphere-atmosphere transfer
353 scheme (BATS) version 1e as coupled to the NCAR Community Climate Model.
354 *Tech.Note NCAR/TN-387+STR, Natl. Center for Atmos. Res., Boulder, Colo.*

355 Dickinson, R.E., Pinty, B., & Verstraete, M.M. (1990). Relating Surface Albedos in Gcm to
356 Remotely Sensed Data. *Agricultural and Forest Meteorology*, 52, 109-131

357 Fensholt, R., Sandholt, I., & Rasmussen, M.S. (2004). Evaluation of MODIS LAI, fAPAR and
358 the relation between fAPAR and NDVI in a semi-arid environment using in situ
359 measurements. *Remote Sensing of Environment*, 91, 490–507

360 Gitelson, A.A. (2004). Wide dynamic range vegetation index for remote quantification of
361 biophysical characteristics of vegetation. *Journal of Plant Physiology*, 161, 165-173

362 Gitelson, A.A., Peng, Y., Masek, J.G., Rundquist, D.C., Verma, S., Suyker, A., Baker, J.M.,
363 Hatfield, J.L., & Meyers, T. (2012). Remote estimation of crop gross primary production
364 with Landsat data. *Rem. Sens. Environ.*, 121, 404-414

365 Gitelson, A.A., Viña, A., J.G., M., Verma, S.B., & Suyker, A.E. (2008). Synoptic Monitoring of
366 Gross Primary Productivity of Maize Using Landsat Data. *IEEE Geoscience and Remote
367 Sensing Letters*, 5, 133-137

368 Gitelson, A.A., Viña, A., Verma, S.B., Rundquist, D.C., Arkebauer, T.J., Keydan, G., Leavitt, B.,
369 Ciganda, V., Burba, G.G., & Suyker, A.E. (2006). Relationship between gross primary
370 production and chlorophyll content in crops: Implications for the synoptic monitoring of
371 vegetation productivity. *J. Geophys. Res.*, 111, D08S11

372 Gitelson, A.A., Wardlow, B.D., Keydan, G.P., & Leavitt, B. (2007). An evaluation of MODIS
373 250-m data for green LAI estimation in crops. *Geophys. Res. Lett.*, 34, L20403

374 Goward, S.N., & Huemmrich, K.F. (1992). Vegetation Canopy PAR Absorptance and the
375 Normalized Difference Vegetation Index - an Assessment Using the SAIL Model.
376 *Remote Sensing of Environment*, 39, 119-140

377 Guindin-Garcia, N., Gitelson, A.A., Arkebauer, T.J., Shanahan, J., & Weiss, A. (2012). An
378 evaluation of MODIS 8- and 16-day composite products for monitoring maize green leaf
379 area index. *Agricultural and Forest Meteorology*, 161, 15– 25

380 Huete, A., Didan, K., Miura, T., Rodriguez, E.P., Gao, X., & Ferreira, L.G. (2002). Overview of
381 the radiometric and biophysical performance of the MODIS vegetation indices. *Remote
382 Sensing of Environment*, 83, 195-213

383 Huete, A.R. (1988). A Soil-Adjusted Vegetation Index (SAVI). *Remote Sensing of Environment*,
384 25, 295-309

385 Huete, A.R., Liu, H.Q., Batchily, K., & vanLeeuwen, W. (1997). A comparison of vegetation
386 indices global set of TM images for EOS-MODIS. *Remote Sensing of Environment*, 59,
387 440-451

388 Jacquemoud, S., & Baret, F. (1990). PROSPECT—a model of leaf optical properties spectra.
389 *Remote Sensing of Environment*, 34, 75–91.

390 Jiang, Z., Huete, A.R., Didan, K., & Miura, T. (2008). Development of a two-band enhanced
391 vegetation index without a blue band. *Rem. Sens. Environ.*, 112, 3833-3845

392 Jin, C., Xiao, X.M., Merbold, L., Arneith, A., Veenendaal, E., & Kutsch, W. (2013). Phenology
393 and gross primary production of two dominant savanna woodland ecosystems in
394 Southern Africa. *Remote Sensing of Environment*, 135, 189-201

395 Kalfas, J., Xiao, X., Vanegas, D., Verma, S., & Suyker, A.E. (2011). Modeling gross primary
396 production of irrigated and rain-fed maize using MODIS imagery and CO(2) flux tower
397 data. *Agricultural and Forest Meteorology*, 151, 1514-1528

398 King, D.A., Turner, D.P., & Ritts, W.D. (2011). Parameterization of a diagnostic carbon cycle
399 model for continental scale application. *Rem. Sens. Environ.*, *115*, 1653-1664

400 Knyazikhin, Y., Martonchik, J.V., Myneni, R.B., Diner, D.J., & Running, S.W. (1998).
401 Synergistic algorithm for estimating vegetation canopy leaf area index and fraction of
402 absorbed photosynthetically active radiation from MODIS and MISR data. *Journal of*
403 *Geophysical Research*, *103*, 32257-32275

404 Knyazikhin, Y., Zhao, M., Nemani, R., Privette, J.L., Shabanov, N., Myneni, R.B., & Running,
405 S.W. (2002). MODIS LAI/FPAR Team Response to BigFoot Validation Results.
406 <http://cybele.bu.edu/modismisr/validation/response.pdf>

407 Li, Z., Yu, G., Xiao, X., Li, Y., Zhao, X., Ren, C., Zhang, L., & Fu, Y. (2007). Modeling gross
408 primary production of alpine ecosystems in the Tibetan Plateau using MODIS images and
409 climate data. *Remote Sensing of Environment*, *107*, 510-519

410 Lyapustin, A., Martonchik, J., Wang, Y., Laszlo, I., & Korkin, S. (2011a). Multi-Angle
411 Implementation of Atmospheric Correction (MAIAC): Part 1. Radiative Transfer Basis
412 and Look-Up Tables. *J. Geophys. Res.*, *116*, D03210

413 Lyapustin, A., Wang, Y., & Frey, R. (2008). An Automatic Cloud Mask Algorithm Based on
414 Time Series of MODIS Measurements. *J. Geophys. Res.*, *113*

415 Lyapustin, A., Wang, Y., Laszlo, I., Hilker, T., Hall, F., Sellers, P., Tucker, J., & Korkin, S.
416 (2012). Multi-Angle Implementation of Atmospheric Correction for MODIS (MAIAC). 3:
417 Atmospheric Correction. *Rem. Sens. Environ.*, *127*, 385-393

418 Lyapustin, A., Wang, Y., Laszlo, I., Kahn, R., Korkin, S., Remer, L., Levy, R., & Reid, J.S.
419 (2011b). Multi-Angle Implementation of Atmospheric Correction (MAIAC): Part 2.
420 Aerosol Algorithm. *J. Geophys. Res.*, *116*, D03211

421 Mahadevan, P., Wofsy, S.C., Matross, D.M., Xiao, X., Dunn, A.L., Lin, J.C., Gerbig, C., Munger,
422 J.W., Chow, V.Y., & Gottlieb, E.W. (2008). A satellite-based biosphere parameterization
423 for net ecosystem CO₂ exchange: Vegetation Photosynthesis and Respiration Model
424 (VPRM). *Global Biogeochemical Cycles*, *22*, GB2005 (2001-2017)

425 Monteith, J.L. (1972). Solar-Radiation and productivity in tropical ecosystems. *Journal of*
426 *Applied Ecology*, *9*, 747-766

427 Monteith, J.L. (1977). Climate and efficiency of crop production in Britain. *Philosophical*
428 *Transaction of the Royal Society of London B: Biological Sciences*, *281*, 277-294

429 Myneni, R.B., Nemani, R.R., & Running, S.W. (1997). Estimation of global leaf area index and
430 absorbed PAR using radiative transfer models. *IEEE TRANSACTIONS ON*
431 *GEOSCIENCE AND REMOTE SENSING*, *35*, 1380-1393

432 Peng, Y., & Gitelson, A.A. (2011). Application of chlorophyll-related vegetation indices for
433 remote estimation of maize productivity. *Agricultural and Forest Meteorology*, *151*,
434 1267- 1276

435 Peng, Y., & Gitelson, A.A. (2012). Remote estimation of gross primary productivity in soybean
436 and maize based on total crop chlorophyll content. *Rem. Sens. Environ.*, *117*, 440-448

437 Peng, Y., Gitelson, A.A., Keydan, G.P., Rundquist, D.C., & Moses, W.J. (2011). Remote
438 estimation of gross primary production in maize and support for a new paradigm based
439 on total crop chlorophyll content. *Remote Sensing of Environment*, *115*, 978-989

440 Peng, Y., Gitelson, A.A., & Sakamoto, T. (2013). Remote estimation of gross primary
441 productivity in crops using MODIS 250 m data. *Rem. Sens. Environ.*, *128*, 186-196

- 442 Potter, C., Klooster, S., Myneni, R., Genovese, V., Tan, P.N., & Kumar, V. (2003). Continental-
443 scale comparisons of terrestrial carbon sinks estimated from satellite data and ecosystem
444 modeling 1982-1998. *Global and Planetary Change*, 39, 201-213
- 445 Potter, C.S., Randerson, J.T., Field, C.B., Matson, P.A., Vitousek, P.M., Mooney, H.A., &
446 Klooster, S.A. (1993). Terrestrial Ecosystem Production - a Process Model-Based on
447 Global Satellite and Surface Data. *Global Biogeochemical Cycles*, 7, 811-841
- 448 Prince, S.D. (1991). A Model of Regional Primary Production for Use with Coarse Resolution
449 Satellite Data. *International Journal of Remote Sensing*, 12, 1313-1330
- 450 Prince, S.D., & Goward, S.N. (1995). Global primary production: A remote sensing approach.
451 *Journal of Biogeography*, 22, 815-835
- 452 Randerson, J.T., Thompson, M.V., Malmstrom, C.M., Field, C.B., & Fung, I.Y. (1996).
453 Substrate limitations for heterotrophs: Implications for models that estimate the seasonal
454 cycle of atmospheric CO₂. *Global Biogeochemical Cycles*, 10, 585-602
- 455 Running, S., Nemani, R., Heinsch, F., Zhao, M., Reeves, M., & Hashimoto, H. (2004). A
456 continuous satellite-derived measure of global terrestrial primary production. *Bioscience*,
457 54, 547-560
- 458 Running, S.W., Thornton, P.E., Nemani, R., & Glassy, J.M. (2000). Global terrestrial gross and
459 net primary productivity from the Earth Observing System. In O.E. Sala, R.B. Jackson,
460 H.A. Mooney & R.W. Howarth (Eds.), *Methods in Ecosystem Science* (pp. 44-57). New
461 York: Springer Verlag
- 462 Schubert, P., Lagergren, F., Aurela, M., Christensen, T., Grelle, A., Heliasz, M., Klemetsson, L.,
463 Lindroth, A., Pilegaard, K., Vesala, T., & Eklundh, L. (2012). Modeling GPP in the
464 Nordic forest landscape with MODIS time series data—Comparison with the MODIS
465 GPP product. *Rem. Sens. Environ.*, 126, 136-147
- 466 Sellers, P. (1987). Canopy reflectance, photosynthesis, and transpiration, II. The role of
467 biophysics in the linearity of their interdependence. *Rem. Sens. Environ.*, 21, 143-183
- 468 Sellers, P.J., Los, S.O., Tucker, C.J., Justice, C.O., Dazlich, D.A., Collatz, G.J., & Randall, D.A.
469 (1996). A revised land surface parameterization (SiB2) for atmospheric GCMs .II: The
470 generation of global fields of terrestrial biophysical parameters from satellite data.
471 *Journal of Climate*, 9, 706-737
- 472 Sellers, P.J., Mintz, Y., Sud, Y.C., & Dalcher, A. (1986). A Simple Biosphere Model (SIB) for
473 Use within General Circulation Models. *J. Atmos. Sci.*, 43, 505-531
- 474 Sellers, P.J., Tucker, C.J., Collatz, G.J., Los, S.O., Justice, C.O., Dazlich, D.A., & Randall, D.A.
475 (1994). A global 1° by 1° NDVI data set for climate studies. Part 2: The generation of
476 global fields of terrestrial biophysical parameters from the NDVI. *International Journal*
477 *of Remote Sensing*, 15, 3519-3545
- 478 Sims, D.A., Rahman, A.F., Cordova, V.D., Baldocchi, D.D., Flanagan, L.B., Goldstein, A.H.,
479 Hollinger, D.Y., Misson, L., Monson, R.K., Schmid, H.P., Wofsy, S.C., & Xu, L.K.
480 (2005). Midday values of gross CO₂ flux and light use efficiency during satellite
481 overpasses can be used to directly estimate eight-day mean flux. *Agricultural and Forest*
482 *Meteorology*, 131, 1-12
- 483 Sims, D.A., Rahman, A.F., Cordova, V.D., El-Masri, B.Z., Baldocchi, D.D., Bolstad, P.V.,
484 Flanagan, L.B., Goldstein, A.H., Hollinger, D.Y., Misson, L., Monson, R.K., Oechel,
485 W.C., Schmid, H.P., Wofsy, S.C., & Xu, L. (2008). A new model of gross primary
486 productivity for North American ecosystems based solely on the enhanced vegetation
487 index and land surface temperature from MODIS. *Rem. Sens. Environ.*, 112, 1633-1646

488 Sims, D.A., Rahman, A.F., Cordova, V.D., El-Masri, B.Z., Baldocchi, D.D., Flanagan, L.B.,
489 Goldstein, A.H., Hollinger, D.Y., Misson, L., Monson, R.K., Oechel, W.C., Schmid, H.P.,
490 Wofsy, S.C., & Xu, L. (2006). On the use of MODIS EVI to assess gross primary
491 productivity of North American ecosystems. *Journal of Geophysical Research*, *111*, 1-16
492 Sjöström, M., Ardö, J., Eklundh, L., El-Tahir, B.A., El-Khidir, H.A.M., Hellström, M., Pilesjö,
493 P., & Seaquist, J. (2009). Evaluation of satellite based indices for gross primary
494 production estimates in a sparse savanna in the Sudan. *Biogeosciences*, *6*, 129-138
495 Sjöström, M., Ardö, J., Arneth, A., Boulain, N., Cappelaere, B., Eklundh, L., Grandcourt, A.d.,
496 Kutsch, W.L., Merbold, L., Nouvellon, Y., Scholes, R.J., Schubert, P., Seaquist, J., &
497 Veenendaal, E.M. (2011). Exploring the potential of MODIS EVI for modeling gross
498 primary production across African ecosystems. *Rem. Sens. Environ.*, *115*, 1081-1089
499 Suyker, A.E., Verma, S.B., Burba, G.G., & Arkebauer, T.J. (2005). gross primary production and
500 ecosystem respiration of irrigated maize and irrigated soybean during a growing season.
501 *Agricultural and Forest Meteorology*, *131*, 180-190
502 Tucker, C.J. (1979). Red and Photographic Infrared Linear Combinations for Monitoring
503 Vegetation. *Remote Sensing of Environment*, *8*, 127-150
504 Verhoef, W. (1984). Light-scattering by leaf layers with application to canopy reflectance
505 modeling—the SAIL model. *Remote Sensing of Environment*, *16*, 125– 141
506 Verhoef, W. (1985). Earth observation modeling based on layer scattering matrices. *Remote*
507 *Sensing of Environment*, *17*, 165– 178
508 Wolfe, R., Roy, D., & Vermote, E. (1998). The MODIS land data storage, gridding and
509 compositing methodology: Level 2 Grid. *IEEE Transactions on Geosciences and Remote*
510 *Sensing*, *36*, 1324-1338
511 Wu, C., Chen, J.M., Desai, A.R., Hollinger, D.Y., Arain, M.A., Margolis, H.A., Gough, C.M., &
512 Staebler, R.M. (2012). Remote sensing of canopy light use efficiency in temperate and
513 boreal forests of North America using MODIS imagery. *Remote Sensing of Environment*,
514 *118*, 60-72
515 Wu, C., Chen, J.M., & Huang, N. (2011). Predicting gross primary production from the enhanced
516 vegetation index and photosynthetically active radiation: Evaluation and calibration. *Rem.*
517 *Sens. Environ.*, *115*, 3424-3435
518 Wu, C., Niu, Z., & Gao, S. (2010). Gross primary production estimation from MODIS data with
519 vegetation index and photosynthetically active radiation in maize. *Journal of Geophysical*
520 *Research*, *115*, 1-12
521 Wu, W., Wang, S., Xiao, X., Yu, G., Fu, Y., & Hao, Y. (2008). Modeling gross primary
522 production of a temperate grassland ecosystem in Inner Mongolia, China, using MODIS
523 imagery and climate data. *Science in China Series D: Earth Sciences*, *51*, 1-12
524 Xiao, X.M., Hollinger, D., Aber, J., Goltz, M., Davidson, E.A., Zhang, Q., & Moore, B. (2004).
525 Satellite-based modeling of gross primary production in an evergreen needleleaf forest.
526 *Rem. Sens. Environ.*, *89*, 519-534
527 Yan, H., Fu, Y., Xiao, X., Huang, H.Q., He, H., & Ediger, L. (2009). Modeling gross primary
528 productivity for winter wheat–maize double cropping system using MODIS time series
529 and CO₂ eddy flux tower data. *Agriculture, Ecosystems and Environment*, *129*, 391-400
530 Zhang, Q. (2003). Improving estimation of terrestrial gross primary productivity (GPP): retrieval
531 of fraction of photosynthetically active radiation absorbed by chlorophyll (fAPARchl)
532 versus FAPAR. *NASA Earth System Science (ESS) Fellowship Program*

533 Zhang, Q., Cheng, Y.-B., Lyapustin, A.I., Wang, Y., Gao, F., Suyker, A., Verma, S., &
534 Middleton, E.M. (2014a). Estimation of crop gross primary production (GPP):
535 MOD15A2 FPAR versus fAPAR_{chl}. *Remote Sensing of Environment*, 153, 1 - 6

536 Zhang, Q., Cheng, Y.-B., Lyapustin, A.I., Wang, Y., Xiao, X., Suyker, A., Verma, S., Tan, B., &
537 Middleton, E.M. (2014b). Estimation of crop daily gross primary production (GPP): I.
538 Impact of MODIS observation footprint area and Impact of vegetation BRDF
539 characteristics. *Agricultural and Forest Meteorology*, 191, 51-63

540 Zhang, Q., Middleton, E.M., Cheng, Y.-B., & Landis, D.R. (2013). Variations of Foliage
541 Chlorophyll fAPAR and Foliage Non-Chlorophyll fAPAR (fAPAR_{chl}, fAPAR_{non-chl}) at
542 the Harvard Forest. *IEEE Journal of Selected Topics in Applied Earth Observations and
543 Remote Sensing*, 6, 2254-2264

544 Zhang, Q., E. M. Middleton, Y.-B. Cheng, K. F. Huemmrich, B. D. Cook, L. A. Corp, W. P.
545 Kustas, A. L. Russ and J. H. Prueger (2014c). Remote estimation of corn daily gross
546 primary production (GPP): integration of fAPAR_{chl} and PRI. *Agricultural and Forest
547 Meteorology*, in review

548 Zhang, Q., Middleton, E.M., Gao, B.-C., & Cheng, Y.-B. (2012). Using EO-1 Hyperion to
549 Simulate HypsIRI Products for a Coniferous Forest: the Fraction of PAR Absorbed by
550 Chlorophyll (fAPAR_{chl}) and Leaf Water Content (LWC). *IEEE Transactions on
551 Geoscience and Remote Sensing*, 50, 1844-1852

552 Zhang, Q., Middleton, E.M., Margolis, H.A., Drolet, G.G., Barr, A.A., & Black, T.A. (2009).
553 Can a MODIS-derived estimate of the fraction of PAR absorbed by chlorophyll
554 (FAPAR_{chl}) improve predictions of light-use efficiency and ecosystem photosynthesis for
555 a boreal aspen forest? *Remote Sensing of Environment*, 113, 880-888

556 Zhang, Q., Xiao, X.M., Braswell, B., Linder, E., Baret, F., & Moore, B. (2005). Estimating light
557 absorption by chlorophyll, leaf and canopy in a deciduous broadleaf forest using MODIS
558 data and a radiative transfer model. *Remote Sensing of Environment*, 99, 357-371

559 Zhao, M., & Running, S.W. (2008). Remote Sensing of Terrestrial Primary Production and
560 Carbon Cycle. In S. Liang (Ed.), *Advances in Land Remote Sensing* (pp. 423–444):
561 Springer Science Business Media

562
563
564
565
566
567
568
569
570
571
572
573
574
575
576
577

578
579
580
581
582
583
584
585
586
587
588
589
590
591
592
593
594
595
596
597
598
599
600
601
602
603
604
605
606
607
608
609
610
611
612
613
614
615
616
617
618
619

Figure captions

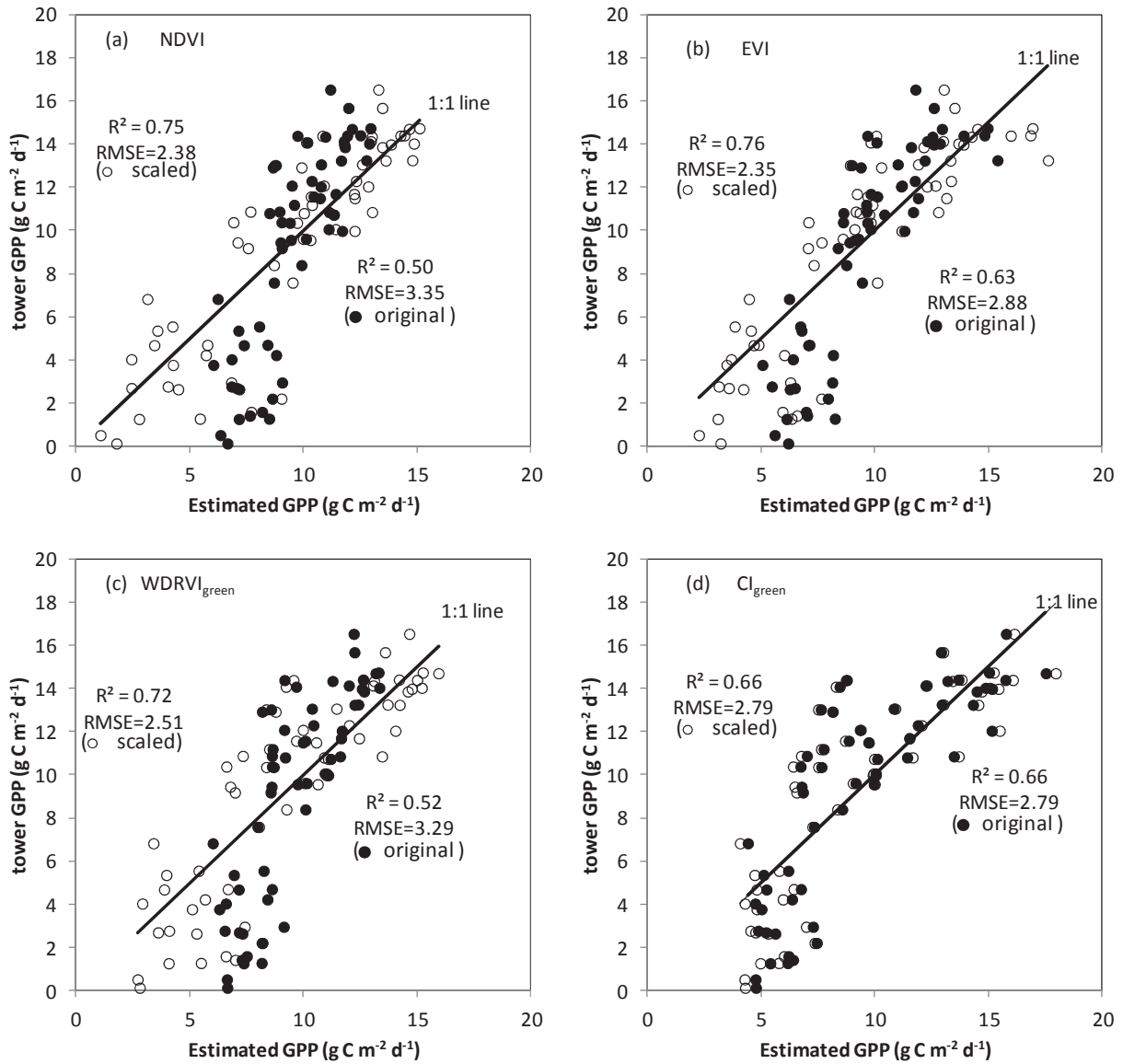
Figure 1. Comparison between tower daily GPP vs. estimated daily GPP for the US-NE3 site (soybean): (a) NDVI; (b) EVI; (c) WDRVI_{green}; and (d) CI_{green}. Filled circles use original unscaled VIs while empty circles use scaled VIs. Only observations with VZA ≤ 35° are included.

Table captions

Table 1. List of relationships between fAPAR_{chl} and VIs for the three crop sites (y=ax+b, y:fAPAR_{chl}, x:VI). The 95% confidence intervals of slope (“a”), y-intercept (“b”), and x-intercept are presented. Coefficients of determination (R²) and root mean square error (RMSE) are also presented.

Table 2. List of the coefficient $\bar{\epsilon}_0$ in $GPP = \bar{\epsilon}_0 * VI * PAR$, the coefficient $\bar{\epsilon}$ in $GPP = \bar{\epsilon} * \text{scaled VI} * PAR$, and LUE_{chl} in $GPP = LUE_{chl} * fAPAR_{chl} * PAR$ (unit: g C mol⁻¹ PPFD)

Table 3. Coefficients of determination (R²), root mean square errors (RMSE, g C m⁻² d⁻¹) and coefficients of variation (CV) for simulated GPP with the VIs using two options: original unscaled VIs versus scaled VIs, compared to tower daily GPP



620
 621 Figure 1. Comparison between tower daily GPP vs. estimated daily GPP for the US-NE3 site
 622 (soybean): (a) NDVI; (b) EVI; (c) WDRVI_{green}; and (d) CI_{green}. Filled circles use original un-
 623 scaled VIs while empty circles use scaled VIs. Only observations with VZA ≤ 35° are included.

624
 625
 626
 627
 628
 629
 630
 631
 632

Table 1. List of relationships between fAPAR_{chl} and VIs for the three crop sites (y=ax+b, y:fAPAR_{chl}, x:VI). The 95% confidence intervals of slope (“a”), y-intercept (“b”), and x-intercept are presented. Coefficients of determination (R²) and root mean square error (RMSE) are also presented.

		NDVI	EVI	WDRVI _{green}	Cl _{green}
US-NE1 (maize, irrigated)	function	y=1.11x-0.29	y=1.30x-0.18	y=1.13x-0.39	y=0.13x-0.13
	slope 95% confidence interval	(1.07, 1.14)	(1.26, 1.34)	(1.09, 1.17)	(0.12, 0.13)
	y intercept 95% confidence interval	(-0.31, -0.27)	(-0.20, -0.17)	(-0.41, -0.37)	(-0.14, -0.11)
	x intercept 95% confidence interval	(0.26, 0.27)	(0.14, 0.15)	(0.34, 0.35)	(0.92, 1.04)
	R ²	0.95	0.96	0.94	0.94
	RMSE	0.06	0.05	0.06	0.06
US-NE2 (maize, irrigated)	function	y=1.10x-0.27	y=1.29x-0.16	y=1.11x-0.37	y=0.12x-0.10
	slope 95% confidence interval	(1.07, 1.14)	(1.25, 1.34)	(1.07, 1.15)	(0.11, 0.12)
	y intercept 95% confidence interval	(-0.29, -0.25)	(-0.18, -0.15)	(-0.40, -0.35)	(-0.12, -0.08)
	x intercept 95% confidence interval	(0.24, 0.25)	(0.12, 0.13)	(0.33, 0.34)	(0.72, 0.91)
	R ²	0.96	0.96	0.95	0.93
	RMSE	0.05	0.05	0.06	0.08
US-NE2 (soybean, irrigated)	function	y=1.06x-0.25	y=1.21x-0.16	y=1.04x-0.32	y=0.11x-0.08
	slope 95% confidence interval	(1.03, 1.10)	(1.18, 1.24)	(1.00, 1.08)	(0.10, 0.12)
	y intercept 95% confidence interval	(-0.27, -0.23)	(-0.17, -0.14)	(-0.34, -0.30)	(-0.10, -0.06)
	x intercept 95% confidence interval	(0.23, 0.24)	(0.12, 0.13)	(0.30, 0.31)	(0.58, 0.81)
	R ²	0.95	0.97	0.94	0.89
	RMSE	0.05	0.05	0.06	0.08
US-NE3 (maize, rainfed)	function	y=1.25x-0.43	y=1.46x-0.25	y=1.13x-0.39	y=0.11x-0.02
	slope 95% confidence interval	(1.12, 1.38)	(1.34, 1.59)	(1.00, 1.26)	(0.10, 0.13)
	y intercept 95% confidence interval	(-0.51, -0.34)	(-0.30, -0.19)	(-0.48, -0.30)	(-0.08, 0.04)
	x intercept 95% confidence interval	(0.33, 0.35)	(0.16, 0.18)	(0.33, 0.36)	(0.05, 0.37)
	R ²	0.82	0.87	0.78	0.73
	RMSE	0.07	0.06	0.07	0.08
US-NE3 (soybean, rainfed)	function	y=1.29x-0.44	y=1.37x-0.24	y=1.07x-0.35	y=0.10x+0.03
	slope 95% confidence interval	(1.18, 1.40)	(1.28, 1.46)	(0.95, 1.19)	(0.08, 0.11)
	y intercept 95% confidence interval	(-0.52, -0.37)	(-0.29, -0.19)	(-0.44, -0.26)	(-0.04, 0.09)
	x intercept 95% confidence interval	(0.33, 0.36)	(0.17, 0.18)	(0.31, 0.35)	(-0.57, -0.02)
	R ²	0.91	0.94	0.85	0.77
	RMSE	0.06	0.05	0.08	0.10

Table 2. List of the coefficient $\bar{\epsilon}_0$ in $GPP = \bar{\epsilon}_0 * VI * PAR$, the coefficient $\bar{\epsilon}$ in $GPP = \bar{\epsilon} * \text{scaled } VI * PAR$, and LUE_{chl} in $GPP = LUE_{chl} * fAPAR_{chl} * PAR$ (unit: $g\ C\ mol^{-1}\ PPFD$)

	LUE_{chl}	NDVI		EVI		WDRVI _{green}		CI _{green}	
		$\bar{\epsilon}_0$	$\bar{\epsilon}$	$\bar{\epsilon}_0$	$\bar{\epsilon}$	$\bar{\epsilon}_0$	$\bar{\epsilon}$	$\bar{\epsilon}_0$	$\bar{\epsilon}$
UE-NE1 (corn, irrigated)	0.65	0.48	0.68	0.65	0.67	0.44	0.68	0.07	0.66
US-NE2 (corn, irrigated)	0.65	0.49	0.66	0.66	0.65	0.45	0.66	0.07	0.65
US-NE2 (soybean, irrigated)	0.42	0.31	0.43	0.40	0.42	0.28	0.43	0.04	0.45
US-NE3 (corn, rainfed)	0.71	0.45	0.73	0.67	0.72	0.43	0.73	0.08	0.72
US-NE3 (soybean, rainfed)	0.43	0.28	0.44	0.39	0.44	0.26	0.44	0.04	0.44

Table 3. Coefficients of determination (R^2), root mean square errors (RMSE, $g C m^{-2} d^{-1}$) and coefficients of variation (CV) for simulated GPP with the VIs using two options: original unscaled VIs versus scaled VIs, compared to tower daily GPP

	NDVI		EVI		WDRVI _{green}		CI _{green}	
	original	scaled	original	scaled	original	scaled	original	scaled
US-NE1	R^2	0.80	0.8	0.88	0.67	0.80	0.77	0.77
	RMSE	4.85	3.77	3.74	2.92	4.88	3.84	4.05
	CV	31%	24%	24%	19%	32%	25%	26%
US-NE2 (corn)	R^2	0.72	0.81	0.83	0.88	0.71	0.77	0.72
	RMSE	4.38	3.62	3.4	2.83	4.42	3.95	4.37
	CV	26%	22%	21%	17%	27%	24%	26%
US-NE2 (soybean)	R^2	0.63	0.78	0.75	0.84	0.65	0.79	0.73
	RMSE	3.16	2.45	2.61	2.11	3.09	2.43	2.76
	CV	31%	24%	26%	21%	30%	24%	27%
US-NE3 (corn)	R^2	0.63	0.80	0.7	0.81	0.62	0.76	0.68
	RMSE	4.66	3.44	4.14	3.32	4.68	3.75	4.31
	CV	33%	25%	30%	24%	34%	27%	31%
US-NE3 (soybean)	R^2	0.5	0.75	0.63	0.76	0.52	0.72	0.66
	RMSE	3.35	2.38	2.88	2.35	3.29	2.51	2.79
	CV	36%	26%	31%	26%	36%	27%	30%